Dalton Transactions

Accepted Manuscript

ROYAL SOCIETY OF CHEMISTRY

www.rsc.org/dalton

Ruthenium Sensitizers Having an Ortho-Dicarboxyl Group as an Anchoring Unit for Dye-Sensitized Solar Cells: Synthesis, Photo- and Electrochemical Properties, and Adsorption Behavior to the TiO_2 Surface

Hironobu Ozawa, Kei Fukushima, Takahito Sugiura, Ayako Urayama and Hironori Arakawa*

Department of Industrial Chemistry, Faculty of Engineering, Tokyo University of Science, 12-1, Ichigaya-Funagawara, Shinjuku, Tokyo, 162-0826, JAPAN
E-mail: h.arakawa@ci.kagu.tus.ac.jp; Fax: (+81) 3 5261 4631; Tel: (+81) 3 5228 831

Abstract

Novel ruthenium sensitizer ((TBA)[Ru(3',4'-dicarboxyterpyridine)$(NCS)_3$], TBA = tetrabutylammonium, **TUS-28**) has been synthesized as an improved model sensitizer for (TBA)[Ru(4'-(3,4-dicarboxyphenyl)terpyridine)$(NCS)_3$] (**TUS-20**). The molar absorptivity of **TUS-28** at the whole visible region was smaller than that of **TUS-20** due to the absence of the phenyl ring at the terpyridine ligand. On the other hand, the energy levels of HOMO and LUMO of **TUS-28** were still suitable for the effective electron transfer reactions in the dye-sensitized solar cells (DSCs). **TUS-28** did not show the superior adsorptivity to the TiO_2 surface just like a **TUS-20**, even though **TUS-28** has an *ortho*-dicarboxyl group which is reported to be an efficient anchoring unit. ATR-IR measurements revealed that both two carboxyl groups of **TUS-28** participate in the binding to the TiO_2 surface the same as **TUS-20**. Therefore, steric hindrance between the hydrogen atom at the 4-position of 3',4'-dicarboxyterpyridine and the OH group at the TiO_2 surface seems to retard the rapid adsorption, and to weaken the binding strength of **TUS-28**. The DSC with **TUS-28** showed 8.2% conversion efficiency, which is higher than that of **TUS-20** (7.5%). *J*sc value of the DSC with **TUS-28** was larger than that of **TUS-20**even though the amount of dye adsorption of **TUS-28** was smaller than that of **TUS-20**. More effective electron injection reaction is considered to contribute mainly to the efficiency improvement of **TUS-28** since the path length of the electron injection from **TUS-28** to the conduction band of the TiO_2 is shorter than that of **TUS-20** due to the absence of the phenyl ring.

Introduction

Extensive studies on the efficiency improvement of dye-sensitized solar cells (DSCs) have been thus far carried out since the pioneering research was reported in 1991.[1]Recently, the light-to-electrical energy conversion efficiency of the DSCs has exceeded 12% by using highly efficient sensitizers such as a polypyridyl ruthenium complex (Z991)[2] or a Zn porphyrin(YD-o-C8).[3]However, further enhancement of the conversion efficiency is required for the industrialization of the DSCs. In this context, continuous efforts have been devoted to develop extremely high-performance sensitizers.[4]The most important requirements for the high-performance sensitizers are both a quite wide absorption with a larger molar absorptivity and the suitable energy levels of HOMO and LUMO. The former enables to utilize whole visible and the near IR light effectively, and the latter enables effective electron transfer reactions in the DSCs such as electron injection from the exited states of dyes into the conduction band of TiO_2, and regeneration of the resulting oxidized forms of dyes by I^-. Moreover, superior adsorptivity and sufficient robustness are also important requirements for the high-performance sensitizers because these features enable quick dye adsorption to the TiO_2 photoelectrodes, and enable to suppress the gradual decrease of the conversion efficiency of the DSCs during the long-term use, respectively. In this regard, various kinds of structural modifications to the previously reported efficient ruthenium sensitizers, such as N719 {$(TBA)_2$[*cis*-Ru$(Hdcbpy)_2(NCS)_2$] (TBA = tetrabutylammonium, dcbpy = 4,4'-dicarboxy-2,2'-bipyridine)} and Black dye {$(TBA)_3$[Ru$(Htcterpy)(NCS)_3$] (tcterpy=4,4',4''-tricarboxy-2,2':6',2''-terpyridine), Figure 1}, have been carried out to develop high-performance sensitizers which satisfies fully the above mentioned requirements. For example, it is reported that introduction of the chromophore units to the bipyridine ligand or terpyridine one increases the molar absorptivity of ruthenium sensitizers effectively,[5] and also reported that utilization of a multidentate ligand instead of monodentate NCS ligands improves the robustness of ruthenium sensitizers.[6]Upon such structural modifications, several high-performance ruthenium sensitizers showing a conversion efficiency higher than that of Black dye have been developed recently.[4j,4k,5j,5k,5l]

On the other hand, continuous efforts have been also devoted in our group for the efficiency improvement of the Black-dye-based DSCs.[7]Recently, 12.0% conversion efficiency was achieved successfully in the cosensitized DSCs with Black dye and D131 by using an electrolyte containing a moderate concentration of a quaternary ammonium iodide.[7f]In addition, structural modifications to Black dye have been thus far carried

out in our group to synthesize high-performance ruthenium sensitizers. Among the ruthenium sensitizers prepared in our group, **TUS-20**having an*ortho*-dicarboxyphenyl group as an anchoring unit (Figure 1) was found to have a superior adsorptivity to the TiO_2 surface. For example, the adsorption rate of **TUS-20**to the TiO_2 surface is faster, and the maximum amount of dye adsorption of **TUS-20** is larger compared to those of Black dye.[8] This superior adsorptivity of **TUS-20** is clearly due to the presence of an*ortho*-dicarboxyphenylgroup. The efficacy of the *ortho*-dicarboxyphenyl group as an anchoring unit to the TiO_2 surface is also demonstrated in the Zn phthalocyanine sensitizer having this anchoring unit.[9] However, the conversion efficiency of the DSC with **TUS-20** was lower than that with Black dye.[8]This inferior performance of **TUS-20** is attributed mainly to the lower incident photon-to-current conversion efficiency (IPCE) at the wavelength range above 650 nm.[8] In addition, promoted backward electron transfer reactions from the conduction band of TiO_2 to the oxidized form of dye and/or to I_3^- in the electrolyte are also considered to be the other reasons for the poor performance of **TUS-20**.[8] Moreover, electron injection yield from the excited state of dye into the conduction band of TiO_2 seems to be lower in the case of **TUS-20** because the path length of this electron transfer reaction is relatively longer due to the presence of the phenyl ring between the terpyridine ligand and the carboxyl anchor. Therefore, relatively lower electron injection yield might be an additional reason for the poor performance of **TUS-20**.

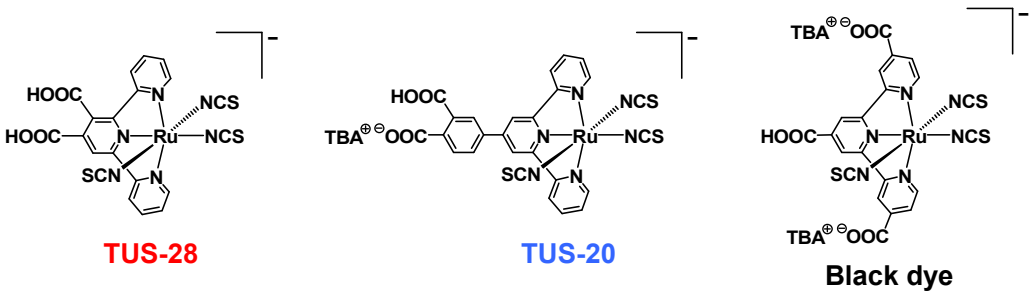

Figure 1. Structures of **TUS-28**, **TUS-20**, and Black dye.

In this study, a novel ruthenium sensitizer with a 3',4'-dicarboxyterpyridine (**TUS-28**) has been synthesized to improve the performance of**TUS-20**. It is expected that **TUS-28** shows a superior adsorptivity to the TiO_2 surface just like a **TUS-20**, and also expected that the electron injection from **TUS-28**to the TiO_2 occurs effectively more than that of **TUS-20** because the path length of the electron injection reaction is shorter. Here we

report synthesis, photo- and electrochemical properties, and the solar cell performances of the DSCs with **TUS-20**and**TUS-28**. Moreover, the adsorption behavior of each sensitizer to the TiO_2 surface, and the interfacial electron transfer dynamics of dye-sensitized TiO_2photoelectrodewill be also reported.

Results and discussion

Synthesis

As reported previously,4'-(3,4-dicarboxyphenyl)terpyridine, which is the ligand of **TUS-20**, was synthesized through a Kröhnke-type reaction and an oxidation of the corresponding dimethyl compound by $KMnO_4$.[8] The total synthetic yield for four steps was about 30%.**TUS-20** was obtained as a TBA salt with a lower yield (ca. 7%) after the multiple purification by a silica gel column chromatography.[8] On the other hand, 3',4'-dicarboxyterpyridine, which is the ligand of **TUS-28**, was synthesized via five steps according to the literature procedure.[10] 3',4'-dicarboxyterpyridine was reacted with $RuCl_3 \cdot 3H_2O$, and further reacted with KNCS in DMF. The crude product was purified on a silica gel column several times using a mixed solvent of CH_3CN, sat. KNO_3aq., and H_2O as an eluent, and then further purified on a HPLC using a TBAOH solution. The pure compound of **TUS-28** was obtained as the same TBA salt (ca. 10%) as **TUS-20**. Both ruthenium sensitizers were characterized successfully by ^1H NMR spectra, EIS-TOF MS and elemental analysis. The amount of TBA^+ contained in **TUS-20** was estimated to be 2.0 from the ^1H NMR spectrum and elemental analysis. Since one TBA^+ exists as a counter cation of **TUS-20**, the other TBA^+ would presence instead of one of the protons of two carboxyl groups at the phenyl ring. In the case of **TUS-28**, the amount of TBA^+ was estimated to be 1.25. Therefore, one of the protons of two carboxyl groups seems to be replaced partially by TBA^+.

Photo- and electrochemical studies

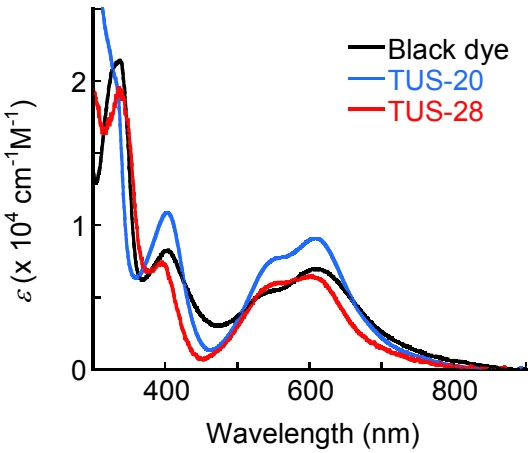

Figure 2. Molar absorptivity spectra of **TUS-28**, **TUS-20** and Black dye in DMF.

Molar absorptivity spectra of **TUS-28**, **TUS-20** and Black dye in DMF are shown in Figure 2. **TUS-28** displayed a quite similar absorption feature to that of Black dye although a small blue shift (ca. 10 nm) of the absorption maxima of two MLCT bands was observed. The molar absorptivity of the band centered at around 400 nm, and that of the MLCT band (500~680 nm) of**TUS-28**was almost equal to that of Black dye. However, the molar absorptivity at the wavelength range between 420 and 500 nm of **TUS-28**were much smaller than that of Black dye. The molar absorptivity of**TUS-20** and (TBA)[Ru(4'-carboxyterpyridine)$(NCS)_3$], which is a structural analog of **TUS-28**,at this wavelength range was also smaller.[5p,11] Therefore, the smaller molar absorptivity between 420 and 500 nm for **TUS-28** and **TUS-20**would be due to the absence of carboxyl groups at the terminal pyridines of the terpyridine ligand. On the other hand, **TUS-20** had a molar absorptivity larger than that of **TUS-28**at the whole visible region. The reason for this improvement in the molar absorptivity of **TUS-20** is considered to be extension of the π-conjugated system of the terpyridine ligand by introducing a phenyl ring. The absorption onset of **TUS-28**wasalmost the same to that of **TUS-20**, and these wavelengths shifted slightly to the shorter wavelength compared to Black dye. These results suggest that the lowest transition energies ($E_{0\text{-}0}$) of **TUS-28**and **TUS-20** are larger than that of Black dye.

Table 1. Electrochemical properties of **TUS-28**, **TUS-20** and Black dye[a]

sensitizer	E_{HOMO} [V vs. SCE]	$E_{0\text{-}0}$[b] [V]	E_{LUMO} [V vs. SCE]
TUS-28	0.66	1.69	-1.03
TUS-20[c]	0.55	1.71	-1.16
Black dye[c]	0.66	1.61	-0.95

[a] All potentials are given vs. SCE. Oxidation potential of **TUS-28** was measured in methanol containing 0.1 M $LiClO_4$. [b] $E_{0\text{-}0}$ was estimated from the intersection wavelength of absorption and luminescence spectra. [c] Data from ref. 8.

Electrochemical property of **TUS-28** was investigated by a cyclic voltammetry in methanol. The quasi-reversible oxidation wave, which is assignable to the Ru(II)/Ru(III) oxidation, was observed at 0.66 V vs. SCE. This value is the same to that of Black dye, and about 0.1 V lower than that of **TUS-20**(Table 1). Since the energy level of HOMO of (TBA)[Ru(4'-carboxyterpyridine)$(NCS)_3$] is reported to be 0.56 V vs. SCE,[5p] introduction of the second carboxyl group to the central pyridine of the terpyridine ligand lowered effectively the energy level of HOMO. On the other hand, $E_{0\text{-}0}$ of **TUS-28** was calculated from the intersection wavelength of the absorption and the luminescence spectra. The obtained value (1.69 eV)was almost equal to that of **TUS-20** (1.71 eV), and larger than that of Black dye (1.61 eV). The estimated energy level of LUMO of **TUS-28** was -1.03 V vs. SCE. The energy levels of HOMO and LUMO of **TUS-28**seem to be suitable for the effective electron injection from the excited state of dye into the conduction band of TiO_2, and the effective reduction of the resulting oxidized form of dye by I^- in the electrolyte.

DFT calculations

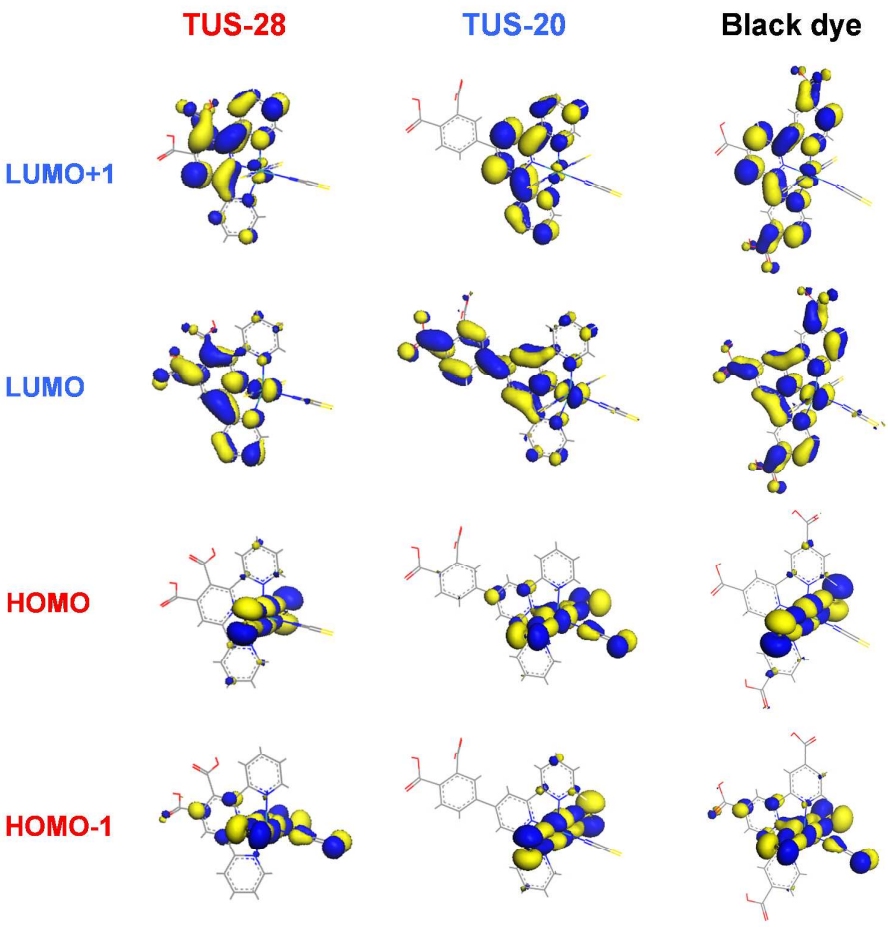

Figure 3. Frontier molecular orbitals (HOMO-1, HOMO, LUMO and LUMO+1) of fully optimized structures of **TUS-28**, **TUS-20**and Black dye in acetonitrile.

Frontier molecular orbitals of**TUS-28** and **TUS-20**, together with those of Black dye are shown in Figure 3. Higher energy HOMOs (HOMO and HOMO-1) of **TUS-28** and **TUS-20**are localized mainly at the Ru(II) atom and two axial NCS ligands. In the case of Black dye, these two molecular orbitals are also populated mainly at the Ru(II) atom and two axial NCS ligands. On the other hand, LUMO of **TUS-28** is delocalized mainly at the central pyridine of 3',4'-dicarboxyterpyridine, and is stabilized largely by the presence of two carboxyl groups (Figure S1). LUMO+1 of **TUS-28** is also delocalized at the central pyridine and one of the terminalpyridines of 3',4'-dicarboxyterpyridine. In the case of **TUS-20**, LUMO is populated at the *ortho*-dicarboxyphenyl unit and the

central pyridine of the terpyridine ligand. LUMO+1 is delocalized over the terpyridine ligand. These results suggest that the electron transfer from the terpyridine unit to the *ortho*-dicarboxyphenyl one, which leads to the electron injection into the conduction band of TiO_2, is thermodynamically favorable. In this case, the path length of this electron transfer reaction is relatively longer due to the presence of the phenyl ring. For comparison, the path length of the electron injection of **TUS-28** is shorter than that of **TUS-20**, therefore, electron injection might occur more effectively in the case of **TUS-28**. On the other hand, LUMO and LUMO+1 of Black dye are delocalized over the terpyridine ligand, therefore, electron injection would proceed effectively.

Adsorption behavior of dyes

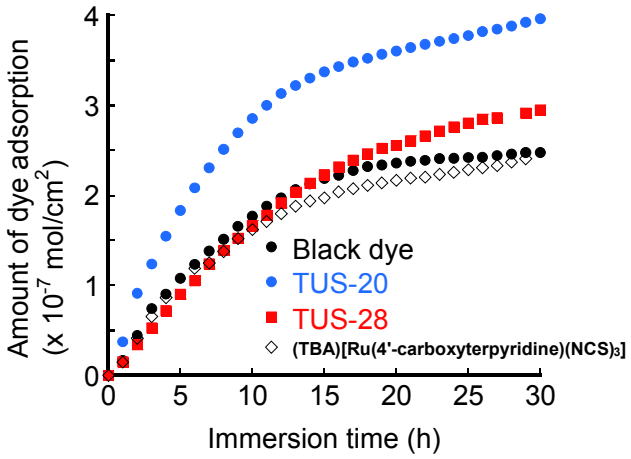

Figure 4. Adsorption profiles of **TUS-28**, **TUS-20**, Black dye and (TBA)[Ru(4'-carboxyterpyridine)(NCS)$_3$] to the TiO_2photoelectrodes at 20 °C.

As reported previously, the adsorption rate of **TUS-20** to the TiO_2 surface is faster, and the maximum amount of dye adsorption is larger compared to those of Black dye.[8]This superior adsorptivity of **TUS-20**must be due to the presence of the *ortho*-dicarboxyphenyl unit. It is expected that **TUS-28** also shows a superior adsorptivity just like a **TUS-20**because **TUS-28** possesses an *ortho*-dicarboxyl group. Therefore, the adsorption behavior of **TUS-28** to the TiO_2 surface, together with that of**TUS-20**, Black dye and (TBA)[Ru(4'-carboxyterpydine)(NCS)$_3$]has been investigated. As shown in Figure 4, the adsorption rate of **TUS-28** was slower than that of **TUS-20**,and the maximum amount of dye adsorption of **TUS-28** was smaller than that of **TUS-20**. The adsorption behavior of **TUS-28** was found to be quite similar to that of Black dye and (TBA)[Ru(4'-carboxyterpyridine)(NCS)$_3$]. On the other hand, almost all adsorbed **TUS-28** could be desorbed from the TiO_2 photoelectrode by immersing the **TUS-28**-adsorbed TiO_2 photoelectrode in a NaOH solution, while some of adsorbed **TUS-20** could not be desorbed from the TiO_2 photoelectrode. In the cases of Black dye and (TBA)[Ru(4'-carboxyterpyridine)(NCS)$_3$], all adsorbed dyes could be desorbed easily by the same treatment. These results indicate that **TUS-28** does not possess a superior adsorptivity to the TiO_2 surface just like a **TUS-20** even though **TUS-28** has an *ortho*-dicarboxyl group as an anchoring unit.

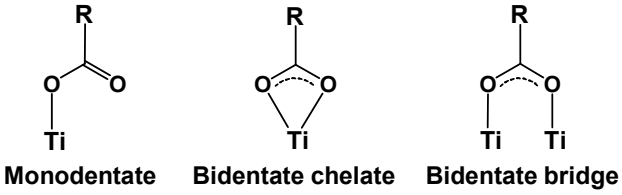

Figure 5. Possible binding modes of the carboxylate anchoring unit at the TiO_2 surface.

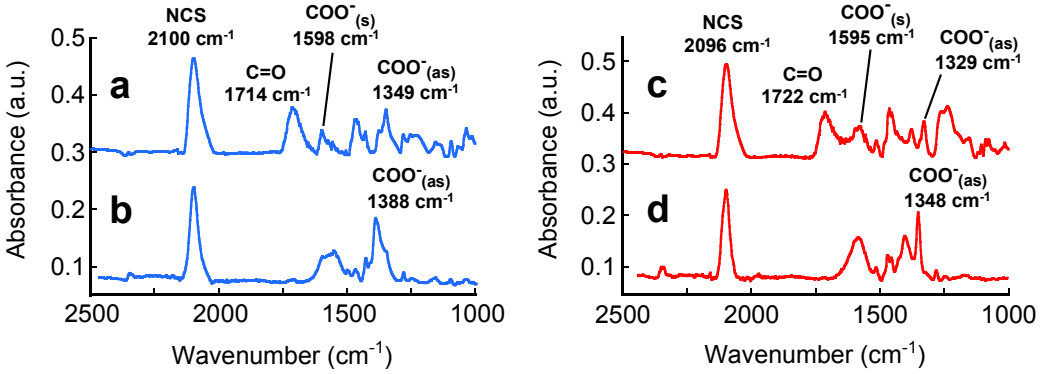

Figure 6. ATR-IR spectra of the powder sample of**TUS-20**(a), **TUS-20** adsorbed on TiO_2nanoparticles(b), powder sample of **TUS-28**(c) and **TUS-28** adsorbed on TiO_2 nanoparticles (d).

In order to know the reasons why **TUS-28** did not have the superior adsorptivity just like a **TUS-20**, ATR-IR measurements of **TUS-28** and **TUS-20** before and after adsorption to the TiO_2surface were conducted. It is noted here that two binding modes of an*ortho*-dicarboxyphenyl unit at the TiO_2 surface have been thus far reported. Imahori and his coworkers reported that one carboxyl group of the *ortho*-dicarboxyphenyl unit binds with a bidentate bridge mode and the other carboxyl group binds with a monodentate mode (Figure 5).[12] On the other hand, Cui, Sun, and their coworkers reported that each carboxyl group of the *ortho*-dicarboxyphenyl unit binds with a bidentate bridge mode to the TiO_2 surface.[13]As shown in Figure 6a, powder sample of **TUS-20**showed the strong absorption at 2100 cm^{-1}, which is assigned

to be the stretching vibration mode of C=N of the N-bounded NCS ligands.[14] Relatively strong absorption band at 1714 cm^{-1} corresponds to the stretching vibration mode of C=O. Two absorption bands at 1598 cm^{-1} and 1349 $cm^{-1}$are attributed to the symmetric and asymmetric stretching vibration modes of COO^-, respectively. The presence of these three bands (ν(C=O), $\nu_s(COO^-)$ and $\nu_{as}(COO^-)$) of the powder sample of **TUS-20** indicates that one of the protons of two carboxyl groups of the *ortho*-dicarboxyphenyl unit of **TUS-20** is replaced by TBA^+, which agrees well with the result of ^1H NMR spectrum as mentioned above. After adsorption to the TiO_2surface, the absorption band of ν(C=O) disappeared completely, and the peak intensity of $\nu_s(COO^-)$ and $\nu_{as}(COO^-)$ increased (Figure 6b). This result indicates that both of two carboxyl groups of **TUS-20**participate in the binding to the TiO_2surface. On the other hand, powder sample of **TUS-28** also showed strong absorption of ν(C=N) of the NCS ligand (2096 cm^{-1}) (Figure 6c). Three absorption bands of ν(C=O), $\nu_s(COO^-)$ and $\nu_{as}(COO^-)$ were also observed at 1722 cm^{-1}, 1595 cm^{-1}, and 1329 cm^{-1}, respectively. Upon the adsorption to the TiO_2 surface, the absorption band of ν(C=O) disappeared completely, and the peak intensity of $\nu_s(COO^-)$ and $\nu_{as}(COO^-)$ increased (Figure 6d). Therefore, two carboxyl groups of **TUS-28** are considered to participate in the binding to the TiO_2 surface just like **TUS-20**.

On the other hand, it is reported that the separation width between the $\nu_s(COO^-)$ band and the $\nu_{as}(COO^-)$ one is one of the criteria for the binding mode of the carboxyl anchoring unit to the TiO_2 surface.[14]For example, binding mode of the carboxyl anchor group is considered to be a monodentate(Figure 5) when the separation width of the dye adsorbed on the TiO_2 surface is equal or larger compared to that of the powder sample of dye.[14] For comparison, the binding mode is considered to be a bidentate chelate or a bidentate bridge (Figure 5) when the separation width of the dye adsorbed on the TiO_2 surface is smaller than that of the powder sample of dye.[14] However, a bidentate chelate is reported to be highly unstable.[14c] Consequently, binding mode of the carboxyl anchor group can be concluded to be a bidetate bridge when the separation width between the $\nu_s(COO^-)$ band and the $\nu_{as}(COO^-)$ one of the dye adsorbed on the TiO_2 surface is smaller than that of the powder sample of dye.[14] In the case of **TUS-20**, the band of $\nu_{as}(COO^-)$ (1349 cm^{-1}) shifted to the higher frequency (1388 cm^{-1}) upon the adsorption to the TiO_2 surface, while the band of $\nu_s(COO^-)$ did not shift. The separation width between the $\nu_s(COO^-)$ band and the $\nu_{as}(COO^-)$ one of the **TUS-20** adsorbed on the TiO_2 surface (210 cm^{-1}) was smaller than that of the powder sample of**TUS-20**(249 cm^{-1}),Therefore, the binding mode of two carboxyl groups of **TUS-20** is considered to a bidentate bridge. On the other hand, the separation width between the $\nu_s(COO^-)$ band

and the $\nu_{as}(COO^-)$ one of the **TUS-28** adsorbed on the TiO_2 surface (247 cm^{-1}) was smaller than that of the powder sample of **TUS-28** (266 cm^{-1}). Therefore, the binding mode of two carboxyl groups of **TUS-28** is also considered to be a bidentate bridge.

These results suggest that **TUS-28** also has the superior adsorptivity just like a **TUS-20**, however, **TUS-28** did not show the superior adsorptivity as mentioned above. One of the possible interpretation is the steric hindrance between the hydrogen atom at the 4-position of 3',4'-dicarboxyterpyridine and the OH group at the TiO_2 surface (Figure 7). In the case of **TUS-20**, such a steric hindrance does not exist due to the presence of the phenyl ring, therefore, the adsorption rate is faster, and the binding to the TiO_2 surface is strong. For comparison, the steric hindrance between the hydrogen atom at the 4-position of 3',4'-dicarboxyterpyridine and the OH group at the TiO_2 surface would exist in the case of **TUS-28**. Therefore, rapid adsorption to the TiO_2 surface was retarded, and the binding strength was weakened even though both carboxyl groups of **TUS-28**bind to the TiO_2 surface with a bidentate bridge mode.

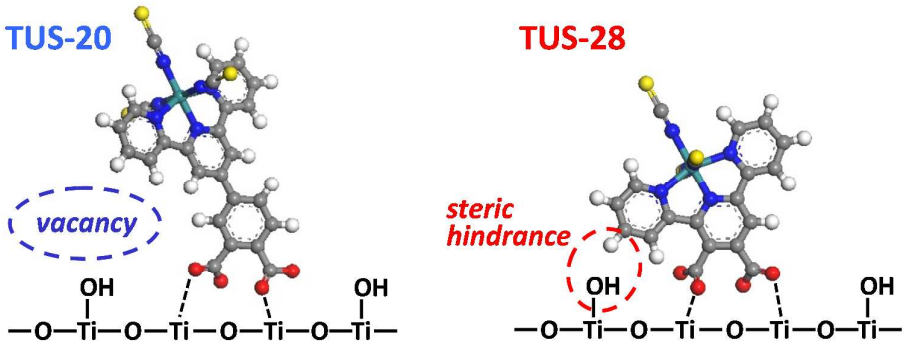

Figure 7. Speculated steric hindrance between the hydrogen atom at the 4-podition of 3',4'-dicarboxyterpyridine of **TUS-28** and the OH group at the TiO_2 surface.

Solar cell performances of the DSCs

Table 2. Solar cell performances of DSCs with **TUS-28**, **TUS-20** and Black dye[a]

Sensitizer	J_{sc} [mA/cm^2]	V_{oc} [V]	*FF*	η [%]	Amount of dye adsorption [$\times 10^{-7}$mol/cm^2]
TUS-28	18.54	0.63	0.70	8.18	2.3
TUS-20	17.19	0.61	0.71	7.47	2.6[b]
Black dye	21.61	0.70	0.72	10.81	2.3

[a] The electrolyte was an acetonitrile solution containing 0.05 M I_2, 0.1 M LiI, 0.6 M DMPImIand 0.3 M TBP. TiO_2 film thickness and active area were ca. 40μm and 0.26 cm^2, respectively. Irradiation was carried out by using the solar simulator (AM 1.5, 100 mW/cm^2). [b] Some amount of adsorbed **TUS-20** could not be desorbed from the TiO_2 photoelectrode.

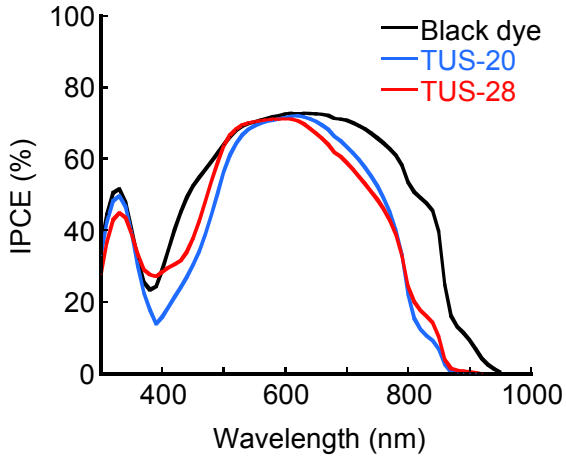

Figure 8. IPCE spectra of the DSCs with **TUS-28**, **TUS-20** and Black dye.

Solar cell performances of the DSCs with **TUS-28**, **TUS-20** and Black dye were summarized in Table 2. The DSCs with **TUS-28** exhibited 8.2% conversion efficiency under the AM 1.5 (100 mW/cm^2) irradiation. This value is higher than that of**TUS-20** (7.5%), even though it is still lower than that of Black dye (10.8%). The J_{sc} value of the DSC with **TUS-28** was larger than that of**TUS-20**, and this improvement of the J_{sc} value contributed mainly to the enhanced conversion efficiency of **TUS-28**. IPCE values of the DSC with **TUS-28** were higher than that obtained in the DSC with **TUS-20** at the whole visible region except for the wavelength range between 600 and 780 nm (Figure 8). The molar absorptivity of **TUS-28**is smaller than that of **TUS-20** at the whole visible

region as mentioned above. In addition, the amount of dye adsorption of **TUS-28** was smaller than that of **TUS-20** (Table 2), although some of adsorbed **TUS-20** could not be desorbed from the TiO_2 photoelectrode due to the superior adsorptivity. Moreover, the energy levels of LUMOs of **TUS-28** and **TUS-20** are sufficient higher for the effective electron injection from the exited state of each dye to the conduction band of TiO_2 as mentioned above. Consequently, the improved performance of **TUS-28** would be attributed to the retardation of the backward electron transfer reactions and/or the improvement of the electron injection yield. On the other hand, the reduction rate of the oxidized form of **TUS-28** by I^- might be faster than that of **TUS-20** because the energy level of HOMO of **TUS-20** is relatively close to the redox potential of I^-/I_3^- couple (ca. 0.2 V vs. SCE). Therefore, more effective regeneration process might be an additional reason for the higher performance of **TUS-28**.

It is noted here that the electron injection yield from the excited state of dye into the conduction band of TiO_2 depends on not only the energy level of LUMO of the sensitizer but also the conduction band energy of TiO_2. The conduction band energy of TiO_2 is known to be lowered by the adsorbed proton which comes from the COOH groups of the sensitizer. Therefore, the amount of adsorbed proton should be also taken into consideration to discuss the electron injection yield. As discussed above, some amount of adsorbed **TUS-20** could not be desorbed from the TiO_2 photoelectrode. However, the actual amount of **TUS-20** adsorption can be estimated from the adsorption profile (Figure 4), which is calculated by the absorbance change of the dye adsorption solvent during the immersion of the TiO_2 photoelectrode. From the Figure 4, the actual amount of **TUS-20** adsorption is estimated to be 3.6×10^{-7}mol/cm^2 after 22 hours immersion. Since the proton of the carboxyl group at the 4-position of the phenyl unit of **TUS-20** is replaced perfectly by TBA^+, the amount of proton contained in **TUS-20** is 1.0. Consequently, the amount of adsorbed proton in the **TUS-20**-adsorbed TiO_2 photoelectrode is considered to be 3.6×10^{-7}mol/cm^2. On the other hand, the amount of **TUS-28** adsorption is calculated to be 2.3×10^{-7}mol/cm^2 as summarized in Table 2. Since one of the protons of two carboxyl groups at the terpyridine ligand is replaced partially by TBA^+ as mentioned above, the amount of proton contained in **TUS-28** is 1.75. Therefore, the amount of adsorbed proton in the **TUS-28**-adsorbed TiO_2 photoelectrode is calculated to be 4.0×10^{-7}mol/cm^2. This value (4.0×10^{-7}mol/cm^2) is only 1.1 times larger than that of the **TUS-20**-adsorbed TiO_2 photoelectrode (3.6×10^{-7}mol/cm^2). Therefore, these results seem to indicate that there is no large difference in the conduction band energies between these two dye-adsorbed TiO_2 photoelectrodes.

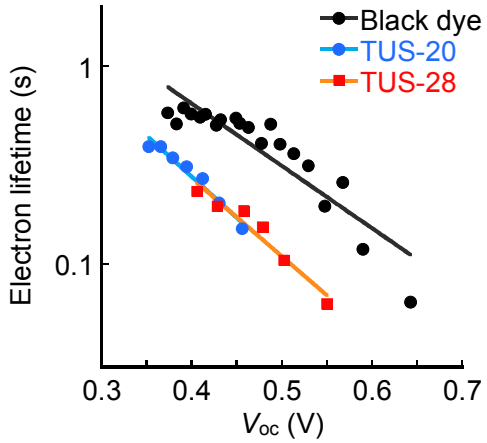

Figure 9. Electron lifetimes as a function of V_{oc} of the DSCs with **TUS-28**, **TUS-20** and Black dye.

Open-circuit voltage decay (OCVD) measurements for the DSCs with **TUS-28**, **TUS-20** and Black dye have been conducted to obtain the insights into the backward electron transfer reactions from the conduction band of TiO_2. In this measurement, injected electrons in the TiO_2 photoelectrode are considered to reduce the oxidized forms of dyes or I_3^-in the electrolyte solution. However, the main pathway would be a reduction ofI_3^- because the oxidized forms of dyes are reduced rapidly by I^- in the electrolyte solution. The electron lifetimes in the TiO_2 photoelectrodes of the DSCs with**TUS-28** and **TUS-20** were found to be much shorter than that of Black dye at the matched V_{oc} value (Figure 9). These results indicate that the backward electron transfer reactions were promoted in the cases of **TUS-28** and **TUS-20** compared to Black dye. On the other hand, the electron lifetimes of **TUS-28**and **TUS-20** were almost equal at the matched V_{oc} value, suggesting that the reaction rates of the backward electron transfer from the TiO_2 to the oxidized form of dye and/or to I_3^- are almost the same in the cases of**TUS-28** and **TUS-20**. Therefore, retardation of the backward electron transfer reactions does not seem to be a major reason for the improved performance of **TUS-28**.

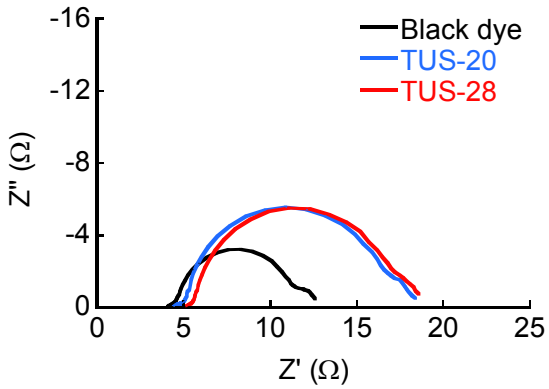

Figure 10. Electrochemical impedance spectra (Nyquist plots) of the DSCs with **TUS-28**, **TUS-20** and Black dye under AM 1.5 irradiation and open-circuit conditions.

Electrochemical impedance spectroscopic (EIS) measurements under the irradiation condition have been carried out to obtain further insights into the internal resistances in the DSCs. As shown in Figure 10, R2 resistances, which correspond to the interfacial resistance at the TiO_2/dye/electrolyte interface, of the DSCs with **TUS-28** and **TUS-20** were much larger than that of Black dye. The observed larger R2 resistances of **TUS-28** and **TUS-20** also indicate that the backward electron transfer reactions were promoted compared to Black dye. In these cases, the major pathway of the backward electron transfer reaction is considered to be an electron transfer from the conduction band of $TiO_2$to I_3^- in the electrolyte solution as the same as OCVD measurements. On the other hand, R2 and the other resistances of the DSCs with **TUS-28** were found to be almost equal to that of **TUS-20**. This result suggests again that there is no remarkable difference in the reaction rates of the backward electron transfer from the TiO_2 to the oxidized form of dye and/or to I_3^- in the electrolyte between the DSCs with **TUS-28** and **TUS-20**. From the OCVD and the EIS measurements, efficiency improvement of **TUS-28** seems to be attributed mainly to the more effective electron injection reaction probably due to the shorter path length of this reaction compared to **TUS-20**.

Nanosecond transient absorption spectroscopy

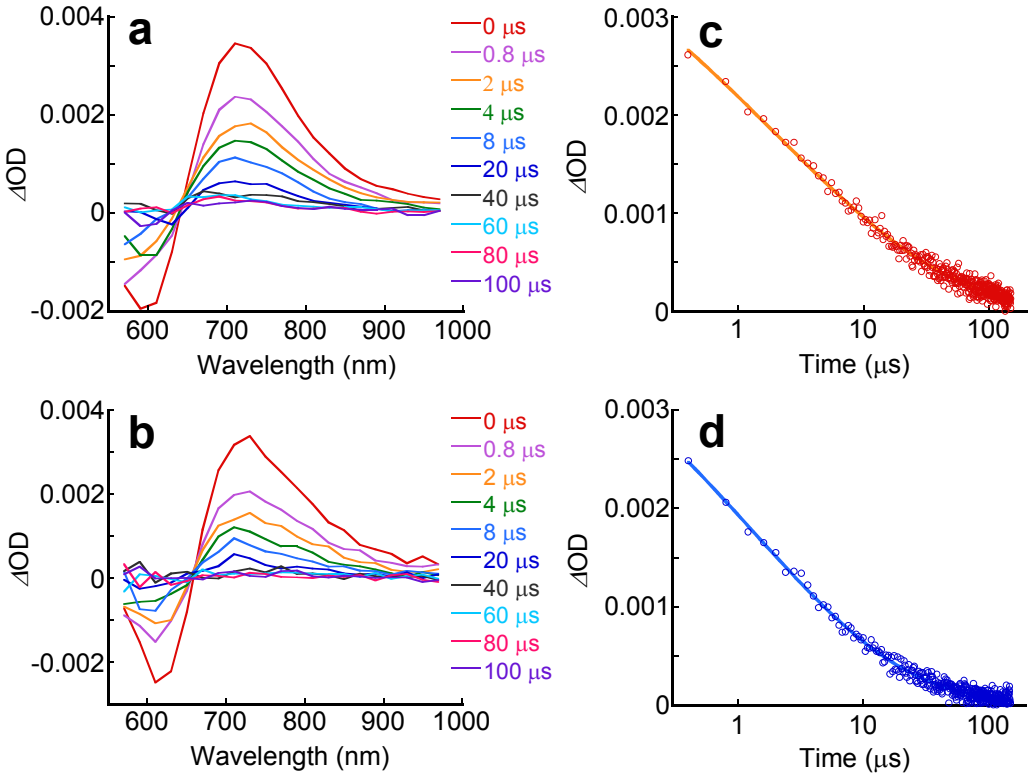

Figure 11. Nanosecond transient absorption spectra of **TUS-28** adsorbed on TiO_2 photoelectrode (a), and that of**TUS-20** adsorbed on TiO_2 photoelectrode (b). The decay profile of **TUS-28** adsorbed on TiO_2 photoelectrode at 730 nm (c), and that of **TUS-20** adsorbed on TiO_2 photoelectrode at 730 nm (d).

Finally, nanosecond transient absorption spectroscopy of the dye-sensitized TiO_2 photoelectrode in the absence of the electrolyte has been conducted to gain further insights into the interfacial electron transfer dynamics. In this experiment, the electron transfer reaction from the conduction band of TiO_2 to I_3^- can be negligible because injected electrons in the TiO_2 photoelectrode can reduce only the oxidized forms of dyes. Therefore, the rate of electron transfer reaction from the conduction band of TiO_2 to the oxidized forms of dyes can be evaluated by this measurement. Figure 11a shows transient absorption spectra of **TUS-28** adsorbed on the TiO_2 photoelectrode in the absence of the electrolyte. Upon the 532 nm laser-pulse excitation, both the bleaching

and the absorption were observed centered at around 590 nm and 730 nm, respectively. The bleaching derives from the loss of the ground state MLCT absorption band, and the absorption corresponds to the absorption band of the oxidized species of **TUS-28**.[14c,15] These bleaching and absorption disappeared perfectly about 60μs after the laser pulse excitation. The decay of the absorption at 730 nm could be fitted well to a stretched exponential function (Figure 11c) the same as previously reported studies on the recombination kinetics between the injected electrons in the TiO_2 photoelectrode and the oxidized forms of dyes.[15a,b,c,e,16] The observed stretched exponential behavior suggests that the electron transport between the trap sites within the TiO_2nanoparticles affects to the recombination reaction between the injected electrons and the oxidized forms of dyes under this condition.[15a,b,c,e,16] The recombination half time ($\tau_{50\%}$) and the stretched exponential dispersion parameter (α) were calculated to be 5 μs and 0.31, respectively. In the case of **TUS-20**, the bleaching and the absorption were also observed centered at around 610 nm and 730 nm, respectively (Figure 11b). The decay at the 730 nm could be also fitted well to a stretched exponential function (Figure 11d). $\tau_{50\%}$ and α were calculated to be 4 μs and 0.35, respectively. These results indicate that the rates of the backward electron transfer reactions from the conduction band of TiO_2 to the oxidized forms of **TUS-28** and **TUS-20** are almost equal. Consequently, the retardation of the backward electron transfer is not a main factor for the superior performance of **TUS-28**.

All the obtained results seem to indicate that the observed efficiency improvement of **TUS-28** is attributed mainly to the more effective electron injection into the conduction band of TiO_2, which is probably due to the shorter path length of this reaction, because the photo- and electrochemical properties and the adsorptivity of **TUS-28**are not improved, and the backward electron transfer reaction is not retarded compared to those of**TUS-20**.

Conclusion

Novel ruthenium sensitizer with a 3',4'-dicarboxyterpyridine (**TUS-28**) has been synthesized as an improved model sensitizer for the previously reported one (**TUS-20**). By removing the phenyl ring between the anchoring unit and the terpyridine ligand, the molar absorptivity of **TUS-28** was decreased at the whole visible region, although the energy levels of HOMO and LUMO were still suitable for the effective electron transfer reactions in the DSC. Against the expectation, **TUS-28** did not show the superior adsorptivity to the TiO_2 surface just like a **TUS-20**, even though **TUS-28** has an *ortho*-dicarboxyl unit as an anchoring one. From the ATR-IR measurements, both carboxyl groups of **TUS-28** were found to participate in the binding to the TiO_2 surface. Therefore, the steric hindrance between the hydrogen atom at the 4-position of 3',4'-dicarboxyterpyridine ligand of **TUS-28** and the OH group at the TiO_2 surface seems to retard the rapid adsorption to the TiO_2 surface, and also seems to weaken the binding strength of **TUS-28**.

The DSC with **TUS-28** showed 8.2% conversion efficiency, which is higher than that with **TUS-20** (7.5%) although it is still lower than that with Black dye (10.8%). In the case of **TUS-28**, *J*sc value was larger than that of **TUS-20** even though the molar absorptivity was smaller at the whole visible region, and the amount of dye adsorption was smaller compared to those of **TUS-20**. OCVD, EIS and nanosecond transient absorption spectroscopic measurements revealed that the reaction rates of the backward electron transfer in the DSCs with **TUS-28** and **TUS-20** are almost equal. Consequently, efficiency improvement of **TUS-28** seems to be attributed mainly to the more effective electron injection probably due to the shorter path length of this reaction. Conversion efficiency could be improved successfully by removing the phenyl ring between the anchoring unit and the terpyridine ligand. This study provides important insights into the molecular design for the high-performance ruthenium sensitizers.

Acknowledgements

This work was supported by the New Energy and IndustrialTechnology Development Organization (NEDO) of Japan. H. O. acknowledges a Grant-in-Aid for young scientist (B)(No. 25810043) from the Ministry of Education, Culture, Sports, Science, and Technology of Japan.

Experimental Section

Materials and general measurements

TUS-20[8], Black dye{$(TBA)_3[Ru(Htcterpy)(NCS)_3]$}[4c], 3',4'-dicarboxy-2,2':6',2''-terpyridine[10]and $(TBA)[Ru(4'\text{-carboxyterpyridine})(NCS)_3]$[11]were prepared according to the literature procedures. Titanium tetraisopropoxide and deoxycholic acid (DCA) were purchased from Tokyo Chemical Industry Co. 1,2-Dimethyl-3-propylimidazolium iodide (DMPImI) was purchased from Shikoku Kasei. 4-*tert*-Butylpyridine (TBP) was purchased from Sigma-Aldrich. All solvents and reagents were of the highest quality available and were used as received.

The elemental analysis was carried out on a Perkin Elmer 2400II elemental analyzer using acetanilide as a standard material. ^{1}H NMR spectra were acquired on a Bruker Bio Spin AVANCE 400M spectrometer, where chemical shifts in CD_3CN and CD_3OD were referenced to internal standard tetramethylsilane. ESI-TOF (electro spray ionization time-of-flight) mass spectra were recorded on a Brucker Micromass focus spectrometer. UV-visible absorption spectra were recorded on a Shimadzu UV-2550 spectrophotometer. Luminescence spectra were recorded on a JASCO FP-6600 spectrofluorophotometer at the room temperature, where the excited wavelength was600nm. Each DMF solution was bubbled with N_2 for at least 15 min prior to the measurement. Electrochemical measurements were carried out in methanol at a sweep rate of 50 mV/s using a glassy carbon disk working electrode, a Pt wire counter electrode, and a Ag wire reference electrode (ca. 200 mV vs. SCE). The supporting electrolyte was 0.1 M $LiClO_4$.ATR-IR spectra were recorded on a Shimadzu IRPrestige-21 spectrometer equipped with a single-reflection ATR accessory (MIRacle with a diamond prism plate).

Nanosecond transient absorption spectroscopy

Nanosecond laser flash photolysis experiments were carried out by an Unisoku TSP-1500M-01TO nanosecond laser flash photolysis system. Each sample was exited with the second-harmonic of aNd:YAG laser (532 nm, ca. 0.3 mJ/cm^2), and transient absorption change was monitored by a halogen lamp. The transmitted light was detected with a Si photodiode array. Transient absorption changes of dye-sensitized TiO_2 thin films (ca. 7μm) were measured in the absence of the electrolyte. The decay was fitted to a traditional stretched exponential function ($\Delta OD = A + B\exp[-(t/\tau)^{\alpha}]$,where α is a

stretched exponential dispersion parameter).

DFT calculations

MO calculation was carried out using the DFT methods implemented in the DMol^3 code package in Materials Studio 5.5 (Accelrys Inc.). Ground-state geometry optimization was performed using the generalized gradient corrected (GGA) function by Perdew, Barke, and Ernzerhof (PBE). Calculations were performed using the double numerical plus polarization (DNP) basis set. The core electrons were treated with DFT semi-core pseudopotentials (DSPPs).

Synthesis

*(TBA)[Ru(3',4'-dicarboxyterpyridine)(NCS)$_3$]·0.25TBA·2H$_2$O(**TUS-28**)*

$RuCl_3 \cdot 3H_2O$ (0.75 mmol, 0.196 g) was dissolved in 100 mL of EtOH. Chloroform solution (100 mL) of 3',4'-dicarboxy-2,2':6',2''-terpyridine[10] (1.8 mmol, 0.67 g) was added to the former solution, and this mixture was refluxed for 4 h under N_2 in the dark. The reaction mixture was evaporated to dryness, and the residue was dissolved in 100 mL of DMF. 40 mL of H_2O containing of KNCS (33 mmol, 3.2 g) was added, and this mixture was refluxed for 30 min under N_2 in the dark. Then, $N(C_2H_5)_3$ (450 mmol, 63 mL) was added to the reaction mixture, and further refluxed for 2 days under N_2 in the dark. The reaction mixture was evaporated to dryness. The residue was once dissolved in a minimum amount of 0.1 M TBAOH solution, and then 0.5 M HCl was added until the precipitate was formed. The obtained solid was purified on a silica gel column using a mixed solvent of CH_3CN, sat. KNO_3 aq., and H_2O (15/1/3, v/v)for 3 or 4 times, and was further purified by HPLC using a TBAOH solution as an eluent. The blue band was collected, and most of the organic solvent was evaporated. 0.5 M HCl was added until the precipitate was formed. Blue precipitate was filtrated, washed with H_2O, and dried in vacuo; 0.17 g (0.19 mmol, 10.3%). ^{1}H NMR (400 MHz, CD_3CN): δ = 9.02 (d, J = 3.0 Hz, 1H), 8.91 (d, J = 4.3 Hz, 1H), 8.70 (s, 1H), 8.45-8.43 (m, 2H), 8.05-7.99 (m, 2H), 7.77-7.71 (m, 2H), 3.09-3.05 (m, 10H), 1.62-1.55 (m, 10H), 1.38-1.28 (m, 10H), 0.97-0.92 (m, 15H). ESI-TOF MS (negative ion, CH_3OH):838.20 m/z ({(TBA)[**M**-H]}$^-$).Anal. Calcd. for[**M**]·1.25TBA·2H$_2$O: C, 51.34; H, 6.46; N, 10.85. Found: C, 51.05; H, 5.93; N, 10.90%.

Preparation of TiO_2 electrode and DSC

TiO_2 pastes were prepared using titanium tetraisopropoxide.[4c] Nanocrystalline TiO_2 photoelectrodes were prepared by screen printing the TiO_2 paste on fluorine-doped SnO_2 conducting glasses (FTO, Nippon Sheet Glass Co., 10 Ω/square). TiO_2 films were composed of seven layers (from the bottom to the third layer: 20 nm TiO_2 particles, the fourth and fifth layers: a 8:2 mixture of 20 nm and 100 nm particles, the sixth layer: a 6:4 mixture of 20 nm and 100 nm particles, and the top layer: 400 nm TiO_2 particles; film thickness: approximately 45μm). TiO_2 photoelectrodes were calcinated at 520 °C after every layer was coated. The active areas of these TiO_2photoelectrode were determined using a KEYENCE VHX-200 digital microscope. The TiO_2 photoelectrodes were immersed in a 1-propanol solution of 0.2 mMBlack dye and 20 mM DCA, 1-propanol solution of 0.2 mM **TUS-28** and 20mM DCA, or an ethanol solution of 0.2mM **TUS-20** and 20 mM DCA for 22 h at room temperature to adsorb dyes onto the TiO_2 surface.

Photoelectrochemical measurements were performed in a two-electrode sandwich cell configuration made up of the dye-adsorbed TiO_2 electrode, a platinum-sputtered counter electrode, a spacer film (50μm), and an electrolyte solution (0.05 M I_2, 0.1 M LiI, 0.6 M DMPImI, and 0.3 M TBP in acetonitrile).**TUS-28** and Black dye were desorbed from the TiO_2photoelectrode by immersing in 0.05 M NaOH solution, and the amount of dye adsorption was estimated from the absorption spectrum of the resulting solution. Some amount of **TUS-20** could not be desorbed from TiO_2 photoelectrode by immersion more than 24 h.

The photocurrent-voltage (*I-V*) characteristics of the DSCs were measured on a Keithley 2400 source meter under irradiation of AM 1.5, 100 mW/cm^2 (1 sun) supplied by a solar simulator (Yamashita Denso, YSS-150A). The incident light intensity was calibrated with a grating spectroradiometer LS-100 (EKO Instruments) and Si photodiode (Bunkoh Keiki). The incident monochromatic photon-to-current conversion efficiency (IPCE) was measured on a PEC-S10 (Peccell Technologies). Electrochemical impedance spectroscopic (EIS) studies were conducted using an electrochemical interface SI 1287 (Solartron) and a frequency response analyzer 1255B (Solartron).

References

(1) B. O'Regan, M. Grätzel, *Nature*, **1991**, *353*, 737-740.

(2) M. Grätzel, *DSC-IC 3*, **2009**.

(3) A. Yella, H.-W. Lee, H. N. Tsao, C. Yi, A. K. Chandiran, M. K. Nazeeruddin, M. Grätzel, *Science*, **2011**, *334*, 629-634.

(4) a) M. K. Nazeeruddin, A. Kay, I. Rodicio, R. Humphry-Baker, E. Müller, P. Liska, N. Vlachopoulos, M. Gräzel, *J. Am. Chem. Soc.*, **1993**, *115*, 6382-6390; b) M. K. Nazeeruddin, S. M. Zakeeruddin, R. Humphry-Baker, M. Jirousek, P. Liska, N. Vlachopoulos, V. Shklover, C.-H. Fischer, M. Gräzel, *Inorg. Chem.*, **1999**, 38, 6298-6305; c) M. K. Nazeeruddin, P. Péchy, T. Renouard, S. M. Zakeeruddin, R. Humphyry-Baker, P. Comte, P. Liska, L. Cevey, E. Costa, V. Shklover, L. Spiccia, G. B. Deacon, C. A. Bignozzi, *J. Am. Chem. Soc.,***2001**, *123*, 1613-1624; d) M. K. Nazeeruddin, F. D. Angelis, S. Fantacci, A. Selloni, G. Viscardi, P. Liska, S. Ito, B. Takeru, M. Grätzel, *J. Am. Chem. Soc.*, **2005**, 127, 16835-16847; e) F. Gao, Y. Wang, D. Shi, J. Zhang, M. Wang, X. Jing, R. Humphyry-Baker, P. Wang, S. M. Zakeeruddin, M. Grätzel, *J. Am. Chem. Soc.*, **2008**, *130*, 10720-10728; f) C.-Y. Chen, M. Wang, J.-Y. Li, N. Pootrakulchote, L. Alibabaei, C. Ngocle, J.-D. Decoppet, J. Tsai, C. Grätzel, C.-G. Wu, S. M. Zakeeruddin, M. Grätzel, *ACS Nano*, **2009**, *10*, 3103-3109; g) Y. Cao, Y. Bai, Q. Yu, Y. Cheng, S. Li, D. Shi, F. Gao, P. Wang, *J. Phys. Chem. C*, **2009**, *113*, 6290-6297;h) A. Abbotto, N. Manfredi, *Dalton Trans.*, **2011**, *40*, 12421-12438;i) K. C. D. Robson, P. G. Bomben, C. P. Berlinguette, *Dalton Trans.*, **2012**, *41*, 7814-7829; j) T. Funaki, H. Funakoshi, O. Kitao, N. Onozawa-Komatsuzaki, K. Kasuga, K. Sayama, H. Sugihara, *Angew. Chem. Int. Ed.*, **2012**, *51*, 7528-7531; k) Y. Numata, S. P. Singh, A. Islam, M. Iwamura, A. Imai, K. Nozaki, L. Han, *Adv. Funct. Mater.*,**2013**, *23*, 1817-1823.

(5) a) P. Wang, C. Klein, R. Humphry-Baker, S. M. Zakeeruddin, M. Gräzel, *J. Am. Chem. Soc.*, **2005**, *127*, 808-809; b) C.-Y. Chen, S.-J. Wu, C.-G. Wu, J.-G. Chen, K.-C. Ho, *Angew. Chem. Int. Ed.*, **2006**, *45*, 5822-5825; c) F. Gao, Y. Wang, J. Zhang, D. Shi, M. Wang, R. Humphry-Baker, P. Wang, S. M. Zakeeruddin, M. Gräzel, *Chem. Commun.*, **2008**, 2635-2637; d) C.-Y. Chen, J.-G. Chen, S.-J. Wu, J.-Y. Li, C.-G. Wu, K.-C. Ho, *Angew. Chem. Int. Ed.*, **2008**, *47*, 7342-7345; e) B.-S. Chen, K. Chen, Y.-H.

Hong, W.-H. Liu, T.-H. Li, C.-H. Lai, P.-T. Chou, Y. Chi, G.-H. Lee, *Chem. Commun.*, **2009**, 5844-5846; f) J.-Y. Li, C.-Y. Chen, J.-G. Chen, C.-J. Tan, K.-M. Lee, S.-J. Wu, Y.-L. Tung, H.-H. Tsai, K.-C. Ho, C.-G. Wu, *J. Mater. Chem.*, **2010**, *20*, 7158-7164; g) J.-J. Kim, H. Choi, S. Paek, C. Kim, K. Lim, M.-J. Ju, H. S. Kang, M.-S. Kang, J. Ko, *Inorg. Chem.*, **2011**, *50*, 11340-11347; h) P. G. Bomben, T. J. Gordon, E. Scott, C. P. Berlinguette, *Angew. Chem. Int. Ed.*, **2011**, *50*, 10682-10685; i) P. G. Bomben, J. Borau-Garcia, C. P. Berlinguette, *Chem. Commun.*, **2012**, *48*, 5599-5601; j) C.-C. Chou, K.-L. Wu, Y. Chi, W.-P. Hu, S. J. Yu, G.-H. Lee, C.-L. Lin, P.-T. Chou, *Angew. Chem. Int. Ed.*, **2011**, *50*, 2054-2058; k) S.-H. Yang, K.-L. Wu, Y. Chi, Y.-M. Cheng, P.-T. Chou, *Angew. Chem. Int. Ed.*, **2011**, *50*, 8270-8274;l) K.-L. Wu, C.-H. Li, Y. Chi, J. N. Clifford, L. Cabau, E. Palomares, Y.-M. Cheng, H.-A. Pan, P.-T. Chou, *J. Am. Chem. Soc.*, **2012**, *134*, 7488-7496;m) M. Kimura, J. Masuo, Y. Tohata, K. Obuchi, N. Masaki, T. N. Murakami, N. Koumura, K. Hara, A. Fukui, R. Yamanaka, S. Mori, *Chem.-Eur. J.*, **2013**, *19*, 1028-1034; n) H. Ozawa, H. Kawaguchi, Y.Okuyama, H, Arakawa, *Chem. Lett.*, **2011**, *40*, 658-660; o) H. Ozawa, H. Kawaguchi, Y.Okuyama, H. Arakawa, *Ambio*, **2012**, *41*, 149-150; p) H. Ozawa, Y. Yamamoto, K. Fukushima, S. Yamashita, H. Arakawa, *Chem. Lett.,* **2013**, *42*, 897-899; q)H. Ozawa, H. Kawaguchi, Y.Okuyama, H. Arakawa, *Eur. J. Inorg. Chem.*, **2013**, 5187-5195.

(6) a) S. H. Wadman, J. M. Kroon, K. Bakker, M. Lutz, A. L. Spek, G. P. M. Klink, G. Koten, *Chem. Commun.*, **2007**, 1907-1909; b) K. Chen, Y.-H. Hong, Y. Chi, W.-H. Liu, B.-S. Chen, P.-T. Chou, *J. Mater. Chem.*, **2009**, *19*, 5329-5335; c) T. Funaki, M. Yanagida, N. Onozawa-Komatsuzaki, K. Kasuga, Y. Kawanishi, M. Kurashige, K. Sayama, H. Sugihara, *Inorg. Chem. Commun.*, **2009**, *12*, 842-845; d) T. Bessho, E. Yoneda, J.-H. Yum, M. Guglielmi, I. Tavernelli, H. Imai, U. Rothlisberger, M. K. Nazeeruddin, M. Grätzel, *J. Am. Chem. Soc.*, **2009**, *131*, 5930-5934; e) W.-C. Chang, H.-S. Chen, T.-Y. Li, N.-M. Hsu, Y. S. Tingare, C.-Y. Li, Y.-C. Liu, C. Su, W.-R. Li, *Angew. Chem., Int. Ed.*, **2010**, *49*, 8161-8164; f) H. Kisserwan, T. H. Ghaddar, *Dalton Trans.*, **2011**, *40*, 3877-3884; g) K. C. D. Robson, B. D. Koivisto, A. Yella, B. Sporinova, M. K. Nazeeruddin, T. Baumgartner, M. Grätzel, C. P. Berlimguette, *Inorg. Chem.*, **2011**, *50*, 5494-5508; h) H. Ozawa, S. Honda, D. Katano, T. Sugiura, H. Arakawa, *Dalton Trans.*, **2014**, *43*, 8026-8036.

(7) a) Z.-S. Wang, T. Yamaguchi, H. Sugihara, H. Arakawa, *Langmuir*, **2005**, *21*, 4272-4276; b) H. Ozawa, M. Awa, T. Ono, H. Arakawa, *Chem. Asian J.*, **2012**, *7*, 156-162; c) H. Ozawa, Y. Okuyama, H. Arakawa, *Dalton Trans.*, **2012**, *41*,

5137-5139; d) H. Ozawa, R. Shimizu, H. Arakawa, *RSC Adv.*, **2012**, *2*, 3198-3200; e) H. Ozawa, Y. Okuyama, H. Arakawa, *RSC Adv.*, **2013**, *3*, 9175-9177; f) H. Ozawa, Y. Okuyama, H. Arakawa, *ChemPhysChem*, **2014**, *15*, 1201-1206.

(8) H. Ozawa, S. Oura, R. Shimizu, H. Arakawa, *Chem. Lett.*, **2012**, *41*, 1406-1408.

(9) M. García-Iglesias, J.-H. Yum, R. Humphry-Baker, S. M. Zakeeruddin, P. Péchy, P. Vázquez, E. Palomares, M. Grätzel, M. K. Nazeeruddin, T. Torres, *Chem. Sci.*, **2011**, *2*, 1145-1150.

(10) J.-C. Raboin, G. Kirsch, M. Beley, *J. Heterocyclic Chem.*, **2000**, *37*, 1077-1080.

(11) G. C. Vougioukalakis, T. Stergiopoulos, G. Kantonis, A. G. Kontos, K. Papadopoulos, A. Stublla, P. G. Potvin, P. Falaras, *J. Photochem. Photophys. A Chem.*, **2010**, *214*, 22-32.

(12) S. Eu, S. Hayashi, T. Umeyama, Y. Matano, Y. Araki, H. Imahori, *J. Phys. Chem.*, *C*, **2008**, *112*, 4396-4405.

(13) Z. Kong, H. Zhou, J. Cui, T. Ma, X. Yang, L. Sun, *J. Photochem. Photobiol., A, Chem.*, **2010**, *213*, 152-157.

(14) a) N. W. Duffy, K. D. Dobson, K. C. Gordon, B. H. Robinson, A. J. McQuillan, *Phys. Chem. Lett.*, **1997**, *266*, 451-455; b) K. S. Finnie, J. R. Bartlett, J. L. Woolfrey, *Langmuir*, **1998**, *14*, 2744-2749; c) A. Vittadini, A. Selloni, F. P. Rotzinger, M. Grätzel,*J. Phys. Chem., B*, **2000**, *104*, 1300-1306; d) C. Bauer, G. Boschloo, E. Mukhtar, A. Hagfeldt, *J. Phys. Chem., B*, **2002**, *106*, 12693-12704; e) M. K. Nazeeruddin, R. Humphyry-Baker, P. Liska,M. Grätzel,*J. Phys. Chem., B*, **2003**, *107*, 8981-8987; f) C. Klein, M.K. Nazeeruddin, D. D. Censo, P. Liska, M. Grätzel,*Inorg.Chem.*, **2004**, *43*, 4216-4226; g) M. K. Nazeeruddin, R. Humphyry-Baker, D. L. Officer, W. M. Campbell, A. K. Burrell, M. Grätzel,*Langmuir*, **2004**, *20*, 6514-6517.

(15) a) S. A. Haque, Y. Tachibana, R. L. Willis, J. E. Moser, M. Grätzel, D. R. Klug, J. R. Durrant, *J. Phys. Chem., B*, **2000**, *104*, 538-547; b) I. Montanari, J. Nelson, J. R. Durrant, *J. Phys. Chem., B*, **2002**, *106*, 12203-12210; c) A. Reynal, A. Forneli, E.

Martines-Ferrero, A. Sánchez-Díaz, A. Vidal-Ferran, B. C. O'Regan, E. Palomares, *J. Am. Chem. Soc.*, **2008**, *130*, 13558-13567; d) A. Hagfldt, G. Boschloo, L. Sun, L. Kloo, H. Pettersson, *Chem. Rev.*, **2010**, *110*, 6595-6663; e) A. Reynal, A. Forneli, E. Palomares, *Energy Environ. Sci.*, **2010**, *3*, 805-812; f) A. Reynal, E. Palomares, *Eur. J. Inorg. Chem.*, **2011**, 4509-4526.

(16) a) Y. Tachibana, J. E. Moser, M. Grätzel, D. R. Klug, J. R. Durrant, *J. Phys. Chem.*, **1996**, *100*, 20056-20062; b) Y. Tachibana, S. A. Haque, I. P. Mercer, J. R. Durrant, D. R. Klug, *J. Phys. Chem., B*, **2000**, *104*, 1198-1205; c) J. N. Clifford, G. Yahioglu, L. R. Milgrom, J. R. Durrant, *Chem. Commun.*, **2002**, 1260-1261; d) J. N. Clifford, E. Palomares, M. K. Nazeeruddin, M. Grätzel, J. Nelson, X. Li, N. J. Long, J. R. Durrant, *J. Am. Chem. Soc.*, **2004**, *126*, 5225-5233; e) J. R. Durrant, S. A. Haque, E. Palomares, *Coord. Chem. Rev.*, **2004**, *248*, 1247-1257; f) M. García-Iglesias, L. Pellejà, J.-H. Yum, D. González-Rodríguez, M. K. Nazeeruddin, M. Grätzel, J. N. Clifford, E. Palomares, P. Vázquez, T. Torres, *Chem. Sci.*, **2012**, *3*, 1177-1184.

TOC

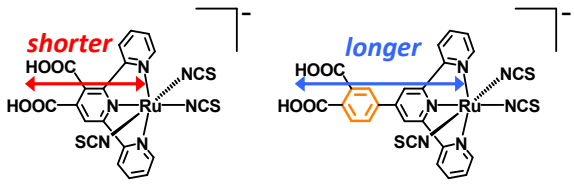

TUS-28 TUS-20

Novel ruthenium sensitizer with a 3',4'-dicarboxyterpyridine (**TUS-28**) has been synthesized as an improved model sensitizer to increase the conversion efficiency of the dye-sensitized solar cells.